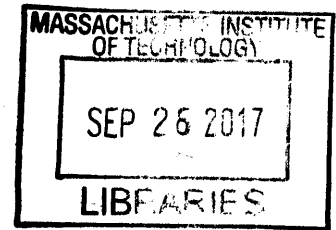


**Photometric and Spectral Analysis
of the Distribution of Crystalline and Amorphous Ices
on Enceladus as Seen by Cassini**

by
Sarah F. Newman



ARCHIVES

Submitted to the Department of Earth, Atmospheric and Planetary Sciences in Partial Fulfillment
of the Requirements for the Degree of

Bachelor of Science in Earth, Atmospheric and Planetary Sciences

at the Massachusetts Institute of Technology

June 9, 2006

© 2006 Sarah F. Newman
All rights reserved

The author hereby grants to M.I.T. permission to reproduce and distribute publicly paper and
electronic copies of this thesis and to grant others the right to do so.

Signature of Author Signature redacted
Department of Earth, Atmospheric and Planetary Sciences

Certified by Signature redacted
Richard Binzel
Thesis Supervisor

Accepted by Signature redacted
Sam Bowring
Chairman of the Department Undergraduate Committee

The author hereby grants to MIT permission to
reproduce and to distribute publicly paper and
electronic copies of this thesis document in
whole or in part in any medium now known or
hereafter created.



77 Massachusetts Avenue
Cambridge, MA 02139
<http://libraries.mit.edu/ask>

DISCLAIMER NOTICE

Due to the condition of the original material, there are unavoidable flaws in this reproduction. We have made every effort possible to provide you with the best copy available.

Thank you.

The following pages were not included in the original document submitted to the MIT Libraries.

This is the most complete copy available.

Photometric and Spectral Analysis of the Distribution of Crystalline and Amorphous Ices on
Enceladus as Seen by Cassini

by

Sarah F. Newman

Submitted to the Department of Earth, Atmospheric and Planetary Sciences on (date) in Partial
Fulfillment of the Requirements for the Degree of
Bachelor of Science in Earth, Atmospheric and Planetary Sciences

Abstract

Photometric and Spectral analysis of data from the Cassini Visual and Infrared Mapping Spectrometer (VIMS) has yielded intriguing findings regarding the properties and composition of the surface of Saturn's satellite Enceladus. Spectral cubes, which contain both spatial and spectral information, were obtained of this satellite with a wavelength distribution in the infrared far more extensive than from any previous observations and at much higher resolution. Using these cubes, we have discovered a distribution of amorphous and crystalline ices on the southern pole of Enceladus, indicating intense ion bombardment in those latitudes and recent geological activity at the "tiger stripe" cracks. Using a composite mosaic of the satellite, we map this distribution of ices according to a "crystallinity factor" and consider investigation of the time scale of the geologic activity based on amorphization rates in the outer solar system.

Thesis Supervisor: Richard Binzel

Title: Professor of Planetary Science

Research Mentor: Bonnie Buratti (Jet Propulsion Laboratories)

Acknowledgements

I'd like to thank my mentor at JPL, Bonnie Buratti, for allowing me to conduct research with her over the past summer and giving me access to this data. I'd also like to thank James Bauer and Tom Momary at JPL for helping me with this work and providing me with models and data. Thank you to Janice Gepner and Eric Newman for editing this paper and to Eric and Mark Newman for technical assistance in analyzing and imaging of this data. Also, thank you to my academic and thesis advisor, Richard Binzel, for all of his guidance during the process of my thesis writing and during my entire undergraduate academic career.

Table of Contents

| | |
|--------------------------------------------------------------------|-------|
| 1. Introduction | pg. 6 |
| 2. Solar System Ices | |
| 2.1 Properties of Amorphous Water Ice..... | 9 |
| 2.2 Amorphous-Crystalline and Amorphous-Amorphous Transitions..... | 10 |
| 2.3 Spectral Characteristics of Amorphous Water Ice..... | 12 |
| 2.4 Amorphous Water Ice in Our Solar System..... | 12 |
| 3. Data..... | 14 |
| 4. Analysis and Discussion | |
| 4.1 Determination of Ice State..... | 16 |
| 4.2 Crystallinity Maps..... | 17 |
| 4.3 Other Indicators of Crystallinity..... | 25 |
| 4.4 Time Scale of Amorphization..... | 26 |
| 5. Conclusion..... | 29 |
| 6. References..... | 30 |

List of Figures

| | |
|-------------------------------------------------------------------------------------------------------------------------------------------------------|----|
| Figure 1. ISS image of Enceladus from the July 14 encounter..... | 7 |
| Figure 2a. CIRS temperature map of Enceladus from July 14 encounter..... | 8 |
| Figure 2b. CIRS temperature map of tiger stripe region of Enceladus from July 14 encounter... | 8 |
| Figure 3. Crystalline and amorphous ice spectra highlighting key bands..... | 15 |
| Figure 4. Crystalline and amorphous water ice spectra in the region of the 3.1 micron band.... | 17 |
| Figure 5. Distribution of crystalline and amorphous ices on Ganymede from Voyager data..... | 18 |
| Figure 6. Crystalline and amorphous water ice spectra (before normalization) and their quadratic continuums in the region of the 3.1 micron band..... | 20 |
| Figure 7. Map showing the Enceladus mosaic in a single band (band 153)..... | 21 |
| Figure 8. Maps of the crystallinity factor on the surface of Enceladus..... | 23 |
| Figure 9. Map of the crystallinity factor on the surface of Enceladus..... | 24 |
| Figure 10. Map of Enceladus showing the depth of the 1.65 micron band..... | 26 |

1. Introduction

The Cassini mission to Saturn has already yielded impressive results in only its first year in orbit. The satellite and its instruments have supplied us with a multitude of images and data of Saturn's system not previously available from ground-based sources and other spacecraft. In addition to the improved spectral resolution of many of Cassini's remote sensing instruments, the spacecraft has obtained data at new phase angles and longitudes and at spatial resolution over an order of magnitude better than that of Voyager. Voyagers I and II explored the Jovian and Saturnian systems in the late 70s and early 80s and continues to travel into the outer reaches of our solar system. This new data coming from Cassini makes it possible to model Saturn, its rings, its magnetosphere and its satellites with much greater accuracy, depth and totality than ever before.

Saturn orbits nearly twice as far from the sun as Jupiter at 9.54 AU and contains a complex system of satellites and rings (Arnett 2005). Between the rings are several gaps most of which are at points of resonance with one or more of Saturn's 34 satellites. The rings, the satellites and Saturn's magnetosphere all have very complicated interactions, justifying the interest in examining this system in the detail made possible by the Cassini-Huygens mission.

Enceladus is one of Saturn's most intriguing icy satellites. It is the brightest object in the solar system with a geometric albedo of 1.04 (Buratti and Veverka 1984), meaning that its surface is covered in pure water ice. It also has craterless regions, implying resurfacing of the satellite. It is located in the middle of a region of maximum concentration of Saturn's E-ring and shows no leading/lagging hemispheric variation (as do all the other satellites in the E-ring), suggesting that

either Enceladus is the source of the E-ring material, or it is somehow able to pick up E-ring particles equally on both hemispheres. Either explanation would have interesting consequences.

On July 14, 2005, Cassini had a targeted encounter of Enceladus with closest approach at 175 km. This encounter revealed many interesting features of the satellite (Figure 1) that were never seen before, such as the “tiger stripes” that flank the south pole, in addition to other unique geologic formations around that region.

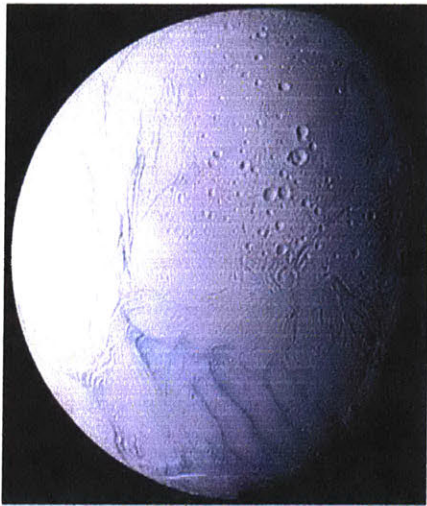


Figure 1. ISS image of Enceladus from the July 14 encounter. Source: <http://saturn.jpl.nasa.gov>

An unexpected hot spot was found on the south pole by the Composite Infrared Spectrometer (CIRS) in the shape of the ridge flanking the region of interesting geology (Figure 2a). This area is 20 K hotter than expected from models of temperature distribution on the satellite, which predict a temperature of 68 K given Enceladus' albedo (Spencer et al. 2006). Upon examination with higher resolution, it is apparent that the latent heat is coming from the tiger stripe cracks, as the variation in temperature between the cracks and the region in between them is upwards of 17 K (Figure 2b). CIRS measured a surface temperature of up to 90 K at the tiger stripes and spectral fitting suggests that the south polar region of Enceladus behaves as a graybody of 133 K (Spencer et al. 2006).

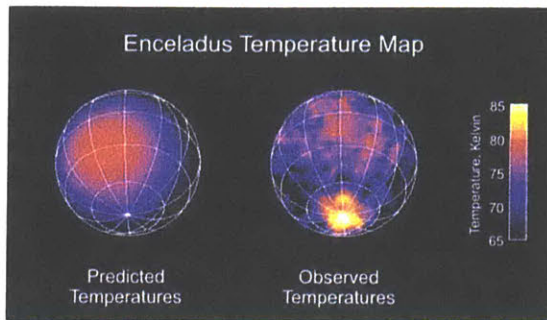


Figure 2a. CIRS temperature map of Enceladus from July 14 encounter.
Source: <http://saturn.jpl.nasa.gov>

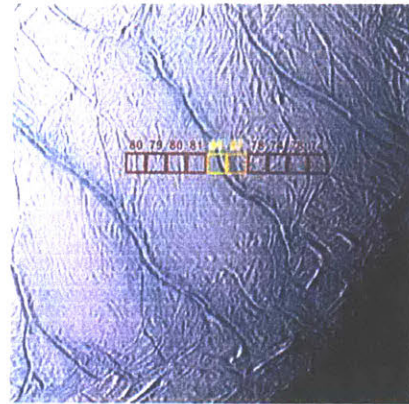


Figure 2b. CIRS temperature map of tiger stripe region of Enceladus from July 14 encounter .
Source: <http://saturn.jpl.nasa.gov>

Using spectral tests for identifying the structural type of water ice, we determined that the south polar region of Enceladus is covered with amorphous ice transformed by high-energy ion bombardment and the tiger stripes are composed of crystalline ice, recrystallized by internal heating below the surface (Brown et al. 2006). While we know that the heating is localized near the south pole of Enceladus and along the tiger stripe cracks, the origin of this heating is as yet unknown. We can predict that as amorphous ice is heated below the surface, it recrystallizes and emerges at the cracks. Over time, the ice will become amorphized by high energy ions diverted towards the poles by Enceladus' magnetosphere. Perhaps this model can be thought of as similar to the processes occurring at mid-ocean ridges on earth. As magma rises to the surface and emerges from the ridges, it cools and undergoes a phase change. Just as we can correlate the age of sea-floor material and the spreading rate at mid-ocean ridges, understanding more about amorphization rates can help us to determine the history of geologic activity on Enceladus. The aim of this paper is to further examine the distribution of crystalline and amorphous ices on the surface of Enceladus using various analytic techniques, specifically the determination of a 'crystallinity factor' in order to better understand these processes.

2. Solar System Ices

Crystalline and amorphous ices exist and are formed under different conditions.

Additionally, certain external or internal forces, such as ion bombardment and internal heating, can cause transitions between the type of ice. It is important to comprehend the properties of these ices and the conditions upon which they can transform to better understand the processes occurring on Enceladus.

2.1 Properties of Amorphous Water Ice

Hexagonal ice or I_h is the most stable form of water below 273 K. At temperatures lower than 180 K, cubic ice I_c , a slightly less stable state of crystalline ice, can form by vapor deposition (Hansen and McCord 2004). The near- and mid-infrared spectrum of I_h and I_c are identical (Devlin 2001). Water vapor deposited at even lower temperatures (< 100 K) or under very low pressures and with rapid cooling will form amorphous states of ice. Amorphous ices are characterized by their lack of structure and definite shape. Their internal structure consists of a random network of hydrogen bonds which leads to short-range ordering (Moore and Hudson 1992). Unless annealed above 100 K, their spectra are highly variable and strongly dependent on the age of the ice and its temperature history (Hansen and McCord 2004). Amorphous ices are important for trapping and releasing volatiles and other guest molecules, and have much lower thermal conductivities and viscosities than their crystalline counterparts (Jenniskens et al. 1998).

There are three key amorphous states at temperatures ($T < 220$ K) and pressures ($P < 0.2$ GPa) relevant for solar system ices: restrained amorphous ice (I_{ar}), low-density amorphous ice (I_{al}) and high-density amorphous ice (I_{ah}). In this temperature/pressure region, transitions between different amorphous states are generally irreversible. Restrained amorphous ice is

formed when water vapor is initially deposited on a very cold surface and then heated to 150 K. It takes the form of cubic crystals embedded in an amorphous matrix. Low-density amorphous ice is formed under colder conditions ($T < 77$ K). High-density amorphous ice requires even colder temperatures ($T < 30$ K) and extremely slow deposition (under 400 microns/hr) to form (Jenniskens et al. 1998).

2.2 Amorphous-Crystalline and Amorphous-Amorphous Transitions

Amorphous ice can form from other states of water ice in several different ways and under certain conditions. Condensation of water vapor on very cold surfaces (77K for $I_{a,l}$ and 30K for $I_{a,h}$) will produce amorphous ice, as will flash freezing of cryovolcanic liquid water (Hansen and McCord 2004). Hexagonal ice can also be transformed into high-density amorphous ice by pressure amorphizing under low temperature conditions (Jenniskens et al. 1998).

Additionally, amorphous ice can be formed from crystalline ice by radiation of high-energy particles, such as ultraviolet photons, helium ions and high-energy electrons. When these particles impinge upon a crystalline ice surface, H_3O^+ , OH^+ , H, OH, and H_2 are produced, disrupting the crystalline structure of hexagonal and cubic ices (Moore and Hudson 1992). Kouchi and Kuroda (1990) found that below 70 K, UV radiation would cause cubic ice to become amorphous. With a flux of 10^{12} photons $cm^{-2} s^{-1}$, crystalline ice between 50 and 70 K would amorphize in 30 minutes to an hour and at 10 K the process would occur much more rapidly. A similar experiment was carried out by Strazzulla et al. (1992) using 3 KeV-helium ions and 1.5 KeV- protons. Crystalline ice was irradiated at several temperatures between 10 and 100 K. The conversion took around one hour, but at $T > 55$ K, the ice was much more resistant to

amorphization. In general, colder temperatures led to faster rates of transformation and the fraction of ice that was converted depended only on the deposited energy and the ice temperature, not on the irradiation rate. Moore and Hudson (1992) repeated this experiment with 700 KeV protons at temperatures between 13 and 77 K. At 77 K, the crystalline water ice became amorphous in 5 hours, and above this temperature, the transformation would not take place. Below 13 K, further bombardment of amorphous water ice would trigger a rapid cycling process between the crystalline and amorphous states. Similarly, Baretta et al. (1991) showed that high-energy ion radiation could trigger partial amorphization of water ice at temperatures up to 80 K, while this process would only occur under 70 K when caused by UV radiation. Lepault, Freeman and Dubochet carried out the same experiment using 100 KeV electrons in 1983 (Moore and Hudson 1992).

Crystalline ice can be formed from amorphous ice by heating, generally above 110-120 K. Modeling has shown that at 115 K, amorphous ice will take one year to become cubic and at 100 K, the transition will take 10 years (Hansen and McCord 2004). In Kouchi and Kuroda's (1990) irradiation experiment, both irradiated and vapor-deposited amorphous ice recrystallized at 146 K in short timescales. A study of ices on comet nuclei noted crystallization of amorphous ice at 137 K for short-pulse warming and even crystallization at 85 K on the scale of one million years (Rickman and Huebner 1990).

The transition between I_{ah} and I_{al} occurs around 40 – 70 K. If amorphous ice remains in its high-density state in solar system bodies long after their formation, the subsequent transition to low-density amorphous ice can cause deep cracks in the interior of the body. Additionally, impure water ice can remain in its amorphous state at higher temperatures than pure water ice. For water ice formed during the birth of our solar system, impure amorphous water ice could still

exist at temperatures up to 90 or 100 K, while pure amorphous water ice could only be present at temperatures up to 72 K (Jenniskens et al. 1998).

2.3 Spectral Characteristics of Amorphous Water Ice

The existence, position, shape, intensity and width of absorption bands in water ice spectra are useful for determining the ice's structure, its crystalline quality, the temperature of the ice and its thermal history. In general, amorphous ice spectra are characterized by wide and relatively unstructured bands. Upon crystallization, ice bands shift to lower wavelengths, become narrower, increase in intensity and often reveal new structures (Schmitt et al. 1998). There are three key bands in the near- to mid-infrared for recognizing amorphous water ice. The 3.1 (3300 cm^{-1}) micron band (O-H stretching mode) can determine the state of ice in the top few microns of the surface of a body. A weak, smooth signature is indicative of cold amorphous ice or warm crystalline ice, whereas a strong, multi-peaked band signals cold crystalline ice. The thin temperature-sensitive absorption band at 1.65 microns is deeper for colder temperatures of crystalline ice, but absent altogether for amorphous ice (Hansen and McCord 2004). There is also a weak 4.53 micron combination mode absorption band which is weaker for amorphous ice (Palumbo 2005). One study showed that the spectrum of crystalline water ice that has been amorphized with radiation resembles something between crystalline ice and vapor deposited amorphous ice (Baratta et al. 1991).

2.4 Amorphous Water Ice in Our Solar System

Amorphous water ice can be found on bodies in the coldest reaches of the solar system and on interstellar dust grains. Most of our solar system's comets were formed at temperatures

below 50 K and still consist mostly of amorphous water ice. However, some can undergo partial crystallization at perihelion and others contain crystalline ice from yet undetermined thermal processes (Moore and Hudson 1992). Amorphous interstellar grains could have formed under temperatures conducive to formation of amorphous water ice or could have been deposited as crystalline ice and subsequently irradiated by cosmic-ray protons and UV photons. With a cosmic ray flux of 4 eV/molecule, half of the ice residing at 50 K would amorphize in 10^6 years (Moore and Hudson 1992). Similarly, with a UV flux of 10^8 photons $\text{cm}^{-2} \text{s}^{-1}$ in diffuse molecular clouds and 10^3 photons $\text{cm}^{-2} \text{s}^{-1}$ in dense molecular clouds, crystalline ice could become amorphous in one and 10^5 years, respectively (Kouchi and Kuroda 1990).

The Near Infrared Mapping Spectrometer (NIMS) aboard the spacecraft Galileo has found amorphous ice in varying amounts on three of Jupiter's larger satellites, Europa, Callisto and Ganymede. The amount of thermal crystallization occurring on these satellites and radiative flux reaching their surfaces varies among them and is reflected in the relative amounts of amorphous vs. crystalline ice on their surfaces. Europa, which receives the largest dose of disruptive radiation, is almost entirely covered in amorphous ice. Callisto, where thermal processes dominate over the radiation flux, is mostly covered in crystalline ice. Ganymede sits between the other two satellites in this balance and contains both amorphous and crystalline ice on its surface. Ganymede's magnetic field is responsible for the distribution of these ices, as it diverts plasma flux to Ganymede's poles, resulting in a greater concentration of amorphous ice at these higher latitudes. However, further detail in the distribution of amorphous ice indicates that there may be other geologic factors affecting the production and distribution of amorphous and crystalline ices on Ganymede (Hansen and McCord 2004).

3. Data

The Visual and Infrared Mapping Spectrometer (VIMS), part of the Remote Sensing palette aboard Cassini, simultaneously obtains data in the form of two-dimensional maps and one-dimensional spectra. This data is stored in 'spectral cubes', three-dimensional data types, such that two dimensions pertain to spatial dimensions and the third is the spectral dimension. Each cube can be used to study brightness variations across a regional surface and also wavelength and spectral differences. Many cubes can be used together to study how brightness varies with solar phase angle (the angle between the body, the observer, and the sun) and sub-spacecraft longitude.

A mosaic of Enceladus' surface was created by Ralf Jaumann of the German Aerospace Center which incorporated VIMS cubes from the 11th Cassini orbit (including images from ENCELADUS_108 to ENCELADUS_111). This mosaic is centered at -50° latitude and 180° longitude and includes the south polar region containing the 'tiger stripes'. The image is composed of 500 x 493 cubes, each with 352 spectral bands. The right edge of Enceladus in the mosaic is not well imaged (it is in a shadow), and therefore, produces noise in the crystallinity maps (Figures 8 and 9). In addition, models of crystalline and amorphous ice spectra created by James Bauer of the Jet Propulsion Laboratories were used in this analysis. Figure 3a shows the model crystalline and amorphous water ice spectra and figure 3b shows characteristic crystalline and amorphous water ice spectra taken from pixels in the mosaic. Both figures show key locations in the spectra for determination of ice state.

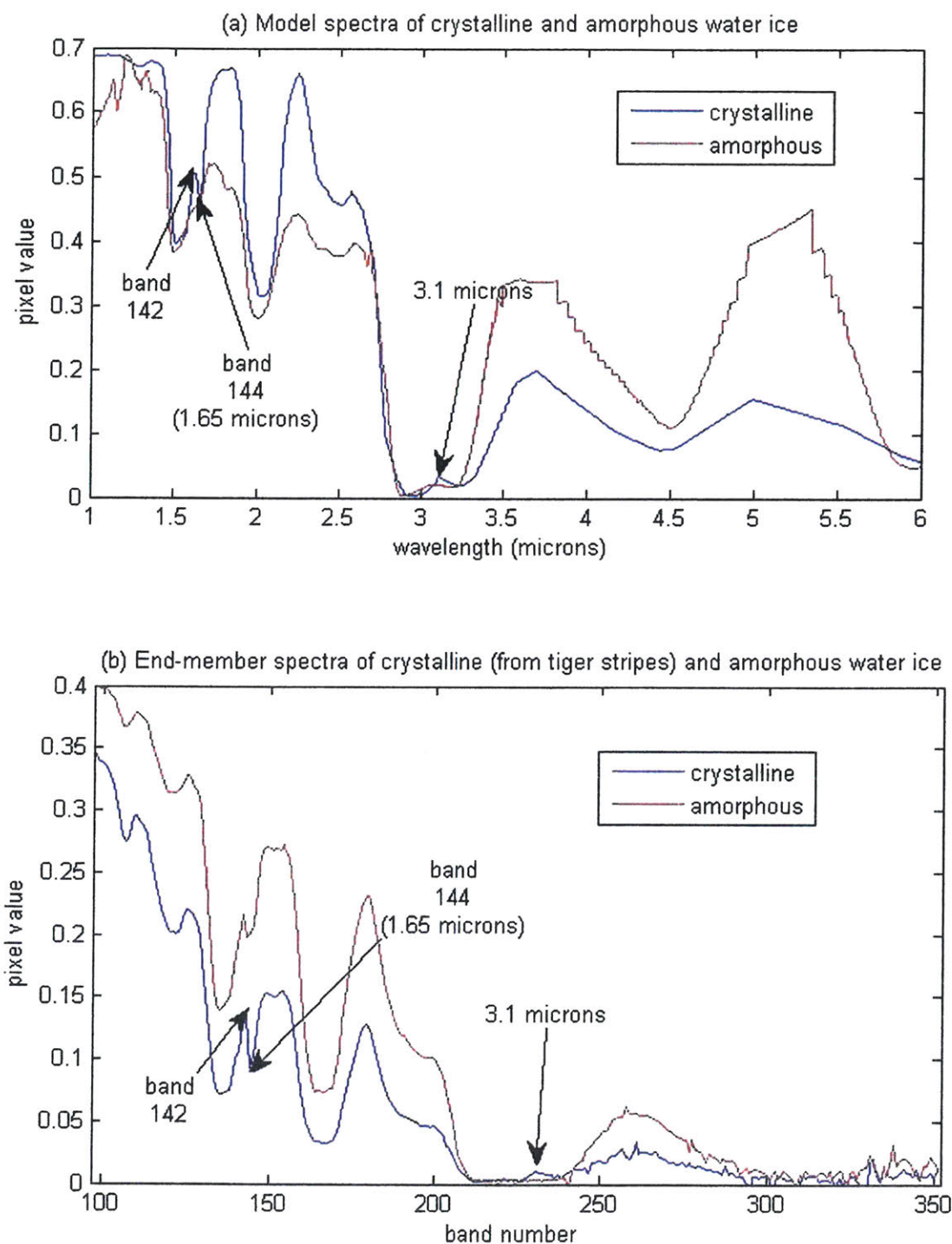


Figure 3. Crystalline and amorphous ice spectra highlighting key bands (specific wavelengths in the spectrum, often the location of absorption or emission). (a) Model spectra from James Bauer (personal communication). (b) End-member spectra made by averaging the spectra from pixels (obtained from the VIMS mosaic constructed with data from Cassini) which displayed crystalline and amorphous characteristics. The crystalline spectrum was made from pixels on the tiger stripes and the amorphous spectrum was made from pixels between the tiger stripes. The corresponding range of wavelengths for this band range is 0.9 – 5.1 microns.

4. Analysis and Discussion

4.1 Determination of Ice State

Several types of evidence are useful for determining the crystalline or amorphous nature of water ice. The individual spectrum of the ice can be compared to laboratory spectra of amorphous and crystalline ice at key wavelengths. In addition looking at the ratioed spectrum of crystalline to amorphous ice can reveal some of the more subtle differences in band position, intensity, width and shape. Individual spectra should be compared at 1.65, 3.1 and 4.53 microns for the aforementioned band characteristics. Of particular interest is the shape of the spectrum in the 3.0 to 3.2 micron region: crystalline spectra show a large peak at 3.1 microns and a sharp decrease to a lower peak at 3.2 microns, whereas amorphous spectra contain a less-structured peak which is more continuous throughout that region (see Figure 4). Analysis of ratioed images (which examines the differences between the bands in crystalline and amorphous ice) and of the 4.53 micron band was carried out in previous work and will not be further investigated here (Brown et al. 2006).

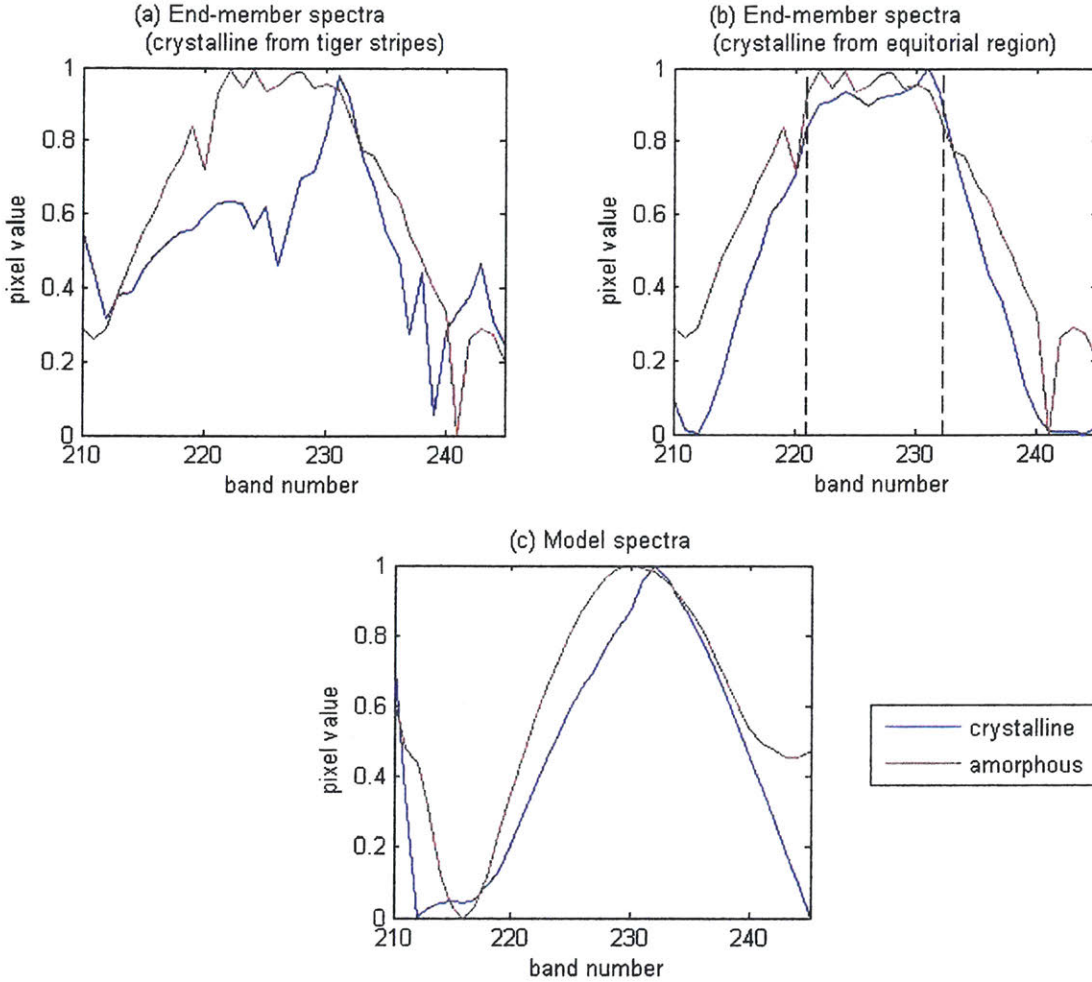


Figure 4. Crystalline and amorphous water ice spectra in the region of the 3.1 micron band. In all of these figures, the quadratic continuum has already been subtracted and the resulting spectrum was normalized between 0 and 1 as described in the next section. Band 232 corresponds to 3.1 microns and band 238 corresponds to 3.2 microns. The crystalline spectra are shown in blue and the amorphous spectra are shown in red. The wavelength range for these figures is 2.75 – 3.33 microns. (a) End-member spectra taken from the mosaic. The crystalline spectrum was made from pixels on the tiger stripes. (b) End-member spectra taken from the mosaic. The crystalline spectrum was taken from pixels in the equatorial region. The dotted lines represent a specific range in the spectrum used to calculate some crystallinity factor maps (see text for details). (c) Model spectra produced by James Bauer.

4.2 Crystallinity Maps

Hansen and McCord (2004) mapped the distribution of ice state across Ganymede by developing an algorithm that determines the ‘crystallinity factor’ for each pixel of the map. The calculation of the crystallinity factor at each point is carried out by comparing a pixel’s spectrum to either model spectra of amorphous and crystalline ice or end-member spectra from the

Ganymede data set. The end-member spectra are spectra averaged from several pixels on the Ganymede map which best display crystalline or amorphous characteristics. For all of these spectra, a cubic continuum is found around the 3.1 micron band and subtracted from the data, which is subsequently normalized between 0 and 1. Subtracting the cubic continuum eliminates elements of the spectrum which are not relevant to this analysis. A linear sum is computed using the model or end-member spectra: $[CF * (\text{crystalline}) + (1 - CF) * (\text{amorphous})]$, where CF is the to-be-determined crystallinity factor and ‘crystalline’ and ‘amorphous’ are the comparative spectra. This sum is found for a range of values of CF (-0.7 to 1.7) and the value (along with the pair of comparative spectra) which produces the best least squares fit for the spectrum of each pixel is that pixel’s CF. Hansen and McCord determined the CF for each pixel of their map of Ganymede and displayed the distribution using false color (Figure 5).

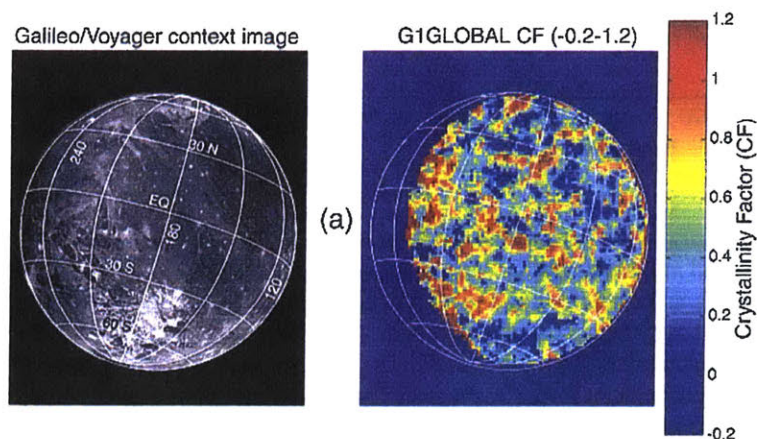


Figure 5. Distribution of crystalline and amorphous ices on Ganymede from Galileo data. The image on the right shows the mapping of the crystallinity factor. Source: Hansen and McCord 2004.

In the present study, a similar technique was used to map the ‘crystallinity factor’ on the surface of Enceladus and maps were constructed displaying this crystallinity factor for the Enceladus mosaic. The crystallinity factor for each pixel of the mosaic was determined by (1) comparing the spectrum of each pixel with model crystalline and amorphous spectra, (2) comparing the spectrum of each pixel with characteristic crystalline and amorphous spectra taken

from the mosaic and (3) the depth of the 1.65 micron band. The characteristic spectra from the mosaic were created by averaging together several spectra that were selected based on visual examination and how well they displayed key elements of crystalline and amorphous water-ice spectra. The characteristic amorphous spectrum was chosen from the area of the south pole adjacent to the tiger stripes. Two different characteristic crystalline spectra were produced, one from pixels in the tiger stripe region and the other from pixels in the equatorial region of Enceladus.

Several different crystallinity maps were produced using the reference spectra. In addition to comparing the spectra of each pixel to three different sets of reference spectra, the analysis was conducted at both the 3.1 and the 1.65 micron regions of the spectrum. The three different sets of reference spectra used were the model crystalline and amorphous spectra and the end-member amorphous spectrum paired with the end-member spectra from both the tiger stripes and the equatorial region of Enceladus. For the 3.1 micron band, the quadratic continuum of the spectra for each pixel (and the model spectra) was found between bands 211 and 244 (corresponding to 2.763 and 3.316 microns). This continuum was subtracted from the spectrum and the spectrum was normalized between 0 and 1 as in the method of Hansen and McCord (2004) (Figure 6). Using the aforementioned linear-sum formula, the crystallinity factor is found for each map by comparing the reference spectra to the pixel's spectrum in the region of the 3.1 micron band and selecting the crystallinity factor which produces the best least squares fit between the sum and the pixel's spectrum. For the 1.65 micron band, the quadratic continuum is found between bands 140 and 148 (1.59 and 1.722 microns) and the least squares computation is carried out in this region.

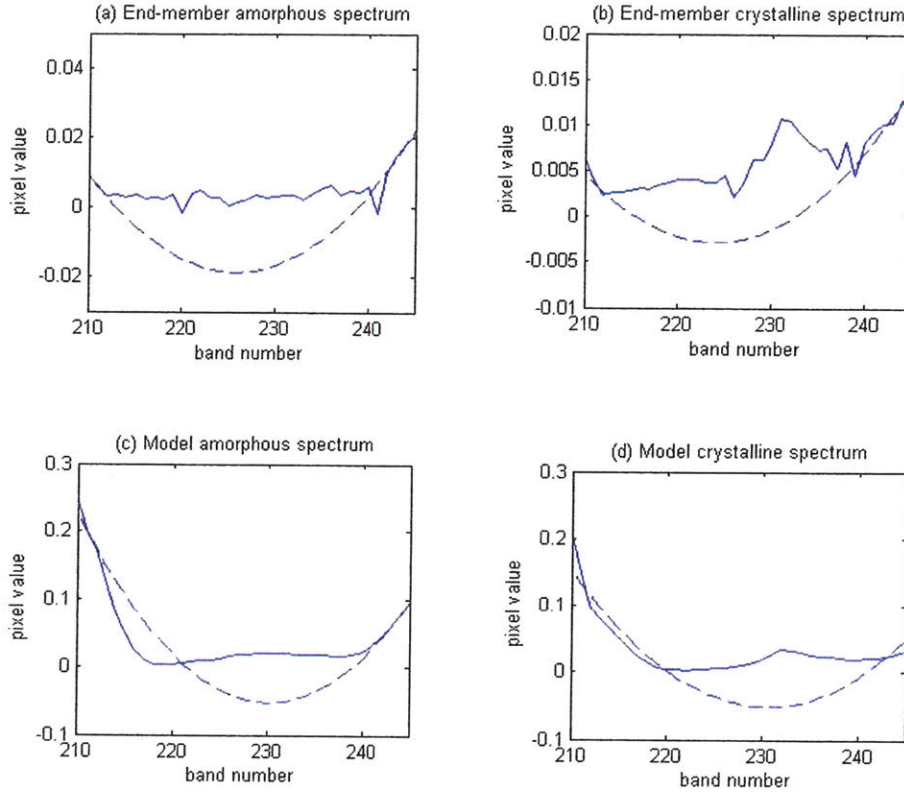


Figure 6. Crystalline and amorphous water ice spectra (before normalization) and their quadratic continuums in the region of the 3.1 micron band. For each of these figures, the quadratic continuum was subtracted and the resulting spectrum normalized to produce the figures in Figure 4. The solid line represents the unnormalized ice spectra and the dotted line represents the quadratic continuum. All of these data were obtained from the Enceladus mosaic. The wavelength range for these figures is 2.75 – 3.33 microns. (a) End-member amorphous spectrum. (b) End-member crystalline spectrum taken from pixels on the tiger stripes. (c) Model amorphous spectrum. (d) Model crystalline spectrum.

Maps were created for each of the three sets of reference spectra from comparison in the region of the 3.1 micron band (Figures 8a-c). In addition, one map was created which used whichever of the sets of spectra produced the best least squares fit for each pixel (Figure 8d). In the four aforementioned maps, there is a dark rectangle which appears on the right side of the tiger stripes. This is an artifact of the data, as the cubes from some of the different observations might not have fit together very well. In order to eliminate this artifact, an additional image was created (using the equatorial crystalline characteristic spectrum) which found the crystallinity factor by comparing the linear sum and each pixel's spectrum in a narrower band range (see the

dotted lines in Figure 4b) which might have eliminated some of the noise (Figure 9). The maps which calculated the crystallinity factor using the 1.65 micron band, proved to be too noisy to be interpretable (this band was not used by Hansen and McCord) and so a map was created instead which showed the distribution of the depth of the 1.65 micron band for each pixel (Figure 10). The aforementioned characteristic was found by subtracting the value of the spectra at band 144 (1.656 microns) from the value at band 142 (1.625 microns). All of the calculations and the initial image processing was done in Matlab. The crystallinity maps were converted to a pseudocolor scale using MetaMorph (Molecular Devices).

In order to ascertain the position of the tiger stripes on the crystallinity maps (Figures 8, 9 and 10) and confirm that they do in fact correspond to a higher crystallinity factor, outlines of the stripes were drawn on a single band map which clearly shows them (Figure 7) and the outlines were superimposed on the crystallinity factor maps.

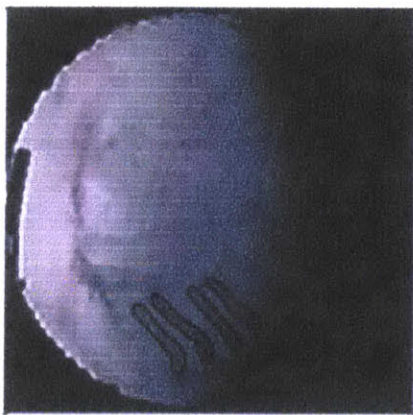


Figure 7. Map showing the Enceladus mosaic in a single band (band 153). The tiger stripes are outlined and these lines were superimposed on the images in Figures 8, 9 and 10.

The crystallinity factor maps in Figure 8 vary to some extent in the overall distribution of crystalline and amorphous ices, but all share a few important characteristics. They all show the tiger stripe region as redder/lighter (more crystalline) than the immediate surrounding region on

the south pole and for the most part, this surrounding region is the bluest/darkest (most amorphous) part of the image. Figure 8a was created using the model crystalline and amorphous spectra as the characteristic spectra and is therefore the least biased towards certain regions (as are the maps using end-member spectra). A portion of the map in the southeastern region is obscured as the mosaic is a composition of many images that were taken under different conditions, with different resolution and with missing data points in parts of the spectrum. However, from this image the aforementioned characteristics (redder on the tiger stripes and bluer around them) are very clear.

Figures 8b and 8c use end-member spectra for their characteristic spectra. Both use a characteristic amorphous spectrum created from pixels in the south polar region between the tiger stripes. For 8b the crystalline spectrum was made from pixels on the tiger stripes and for 8c pixels were chosen in the equatorial region of Enceladus. The maps are slightly biased toward representing certain regions as more crystalline, either the tiger stripes in Figure 8b or the surface outside the south pole for Figure 8c. However, even in the very uniformly bright map of Figure 8c (where the characteristic crystalline spectrum was taken from end-members in the equatorial region) the tiger stripes are visible as redder bands on a bluer background.

Figure 8d is a composition of the other three maps. For each pixel, the set of characteristic spectra that formed a linear combination with the best least squares fit to the pixel's spectrum was used to determine the crystallinity factor. Since the resulting image was so bright that it was difficult to discern relatively brighter and darker regions, a factor of 0.2 was subtracted from the value of the crystallinity factor for each pixel. Perhaps this image most clearly displays the distribution of crystalline and amorphous ice. The tiger stripes (which we

believe to be producing fresh crystalline ice) are the reddest, the south polar region around the stripes are bluer and the surrounding areas are relatively red.

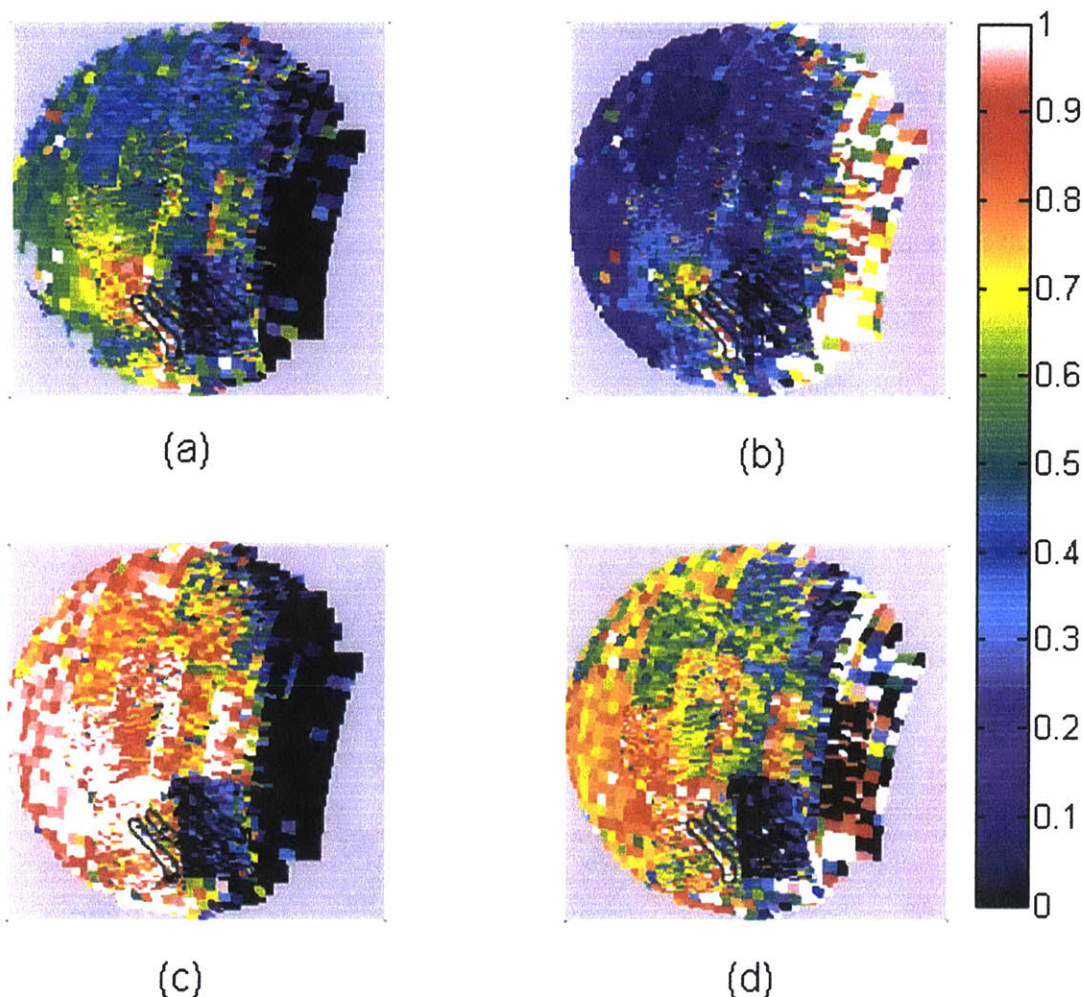


Figure 8. Maps of the crystallinity factor on the surface of Enceladus. Lighter/redder color denotes a higher crystallinity factor (crystalline ice) and darker/bluer color represents a lower crystallinity factor (amorphous ice). All of these maps were constructed by comparing each pixel's spectrum and a set of characteristic crystalline and amorphous spectra in the region of the 3.1 micron band. The black outlines (lower center) represent the border of the tiger stripes as discerned from a single band image of the mosaic (Figure 7) and superimposed on these images. (a) Map created by using the model spectra as the characteristic spectra. (b) Map created using the end-member amorphous spectrum and the end-member crystalline spectrum made from pixels on the tiger stripes as the characteristic spectra. (c) Map created using the end-member amorphous spectrum and the end-member crystalline spectrum made from pixels in the equatorial region as the characteristic spectra. (d) Map created using all three sets of characteristic spectra. For each pixel, the pair of spectra that had the best least squares fit was used to determine the crystallinity factor. A factor of 0.2 was subtracted from the value of each pixel to make the image easier to analyze (it was very saturated).

Figure 9 is a crystallinity map that was created to eliminate some of the noise present in the other maps. It was created using the end-member amorphous spectrum and the end-member crystalline spectrum from the equatorial region. The crystallinity factor for each pixel was determined using a narrower range of bands (bands 121 – 133) around the 3.1 micron region and thus could potentially eliminate some noise. Even though the end-member crystalline spectrum was taken from the equatorial region and not the tiger stripes (as in Figure 8c), the stripes themselves are still very red/light and the region between them is much bluer/darker. However, the region immediately outside the tiger stripes is represented as much more crystalline in this map than in the others.

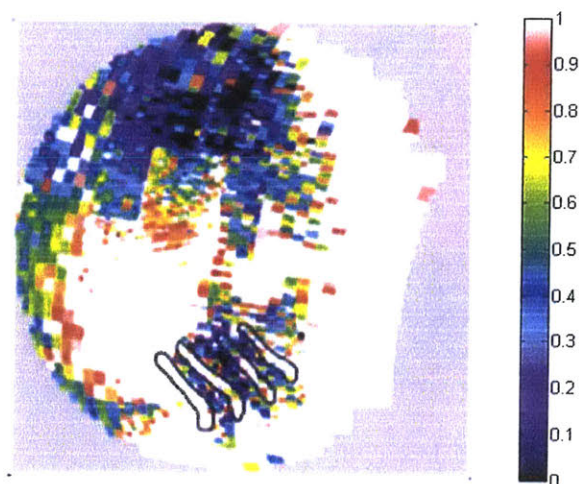


Figure 9. Map of the crystallinity factor on the surface of Enceladus. This map uses the amorphous end-member spectrum and the crystalline end-member spectrum taken from the equatorial region. The crystallinity factor was determined using a narrower range of the spectrum surrounding the 3.1 micron region. The black outlines denote the border of the tiger stripes as determined from the image in Figure 7. In this image, lighter/redder areas are more crystalline and darker/bluer areas are more amorphous.

It should be noted that to create these crystallinity maps, a quadratic continuum was subtracted from each spectrum (see Figure 6) as opposed to a cubic continuum as in the case of

Hansen and McCord's crystallinity maps (2004). A cubic continuum was first attempted, but the resulting fits did not accurately match the shape of the spectra in the region of interest.

4.3 Other Indicators of Crystallinity

The depth of the 1.65 micron band is also a good indicator of crystallinity. This band is almost nonexistent in amorphous ice (it generally only appears in amorphous ice that was deposited in a crystalline form and was subsequently amorphized by bombardment) (Baratta et al. 1991). In addition, the band is temperature-sensitive, such that it is deeper for colder crystalline ice. Thus in a map of the depth of this band, we would expect to see areas of cold crystalline ice as the brightest, followed by areas of warm crystalline ice and then amorphous ice. Figure 10 shows a map of the depth of this band and agrees well with the crystallinity maps. The darkest part of the image is the region in between the tiger stripes (even though the tiger stripes themselves have the smallest average signal), the stripes are brighter and the remaining surface of Enceladus is the brightest. This is consistent with a model in which most of Enceladus is crystalline, the poles are largely amorphous and the tiger stripes are hot regions where the surrounding amorphous ice is recrystallized. A crystallinity map based on the 1.65 micron band is not very useful as the property that distinguishes the type of ice is the depth of the band and not the shape. Upon normalization, this characteristic would disappear and all of the spectra would look more or less the same in the region of the band.



77 Massachusetts Avenue
Cambridge, MA 02139
<http://libraries.mit.edu/ask>

DISCLAIMER NOTICE

MISSING PAGE(S)

26-30

- Moore, M., Hudson, R. and Gerakines, P., (2001), Mid- and far-infrared spectroscopic studies of the influence of temperature, ultraviolet photolysis and ion irradiation on cosmic-type ices, *Spectrochimica Acta Part A*, 57, 843-858.
- Palumbo, M., (2005), The morphology of interstellar water ice, *Journal of Physics: Conference Series*, 6, 211-216.
- Rickman, H. and Huebner, W. (1990), Comet formation and evolution in *Physics and Chemistry of Comets*. ed. Huebner, W. Berlin: Springer-Verlag.
- Schmitt, B. et al. (1998), Optical Properties of ices from UV to infrared in *Solar System Ices*. ed. Schmitt, B. Boston: Kluwer Academic Publishers.
- Spencer, J. et al. (2006), Cassini Encounters Enceladus: Background and the Discovery of a South Polar Hot Spot, *Science*, 311, 1401-1405.
- Strazzulla, G., G. Baratta, G. Leto, and G. Foti, (1992), Ion-beam-induced amorphization of crystalline water ice, *Europhysics Letters*, 18, 517-522.
- Passage to a Ringed World. ed. Spilker, L. NASA, 1997.
- Amorphous Ice and Glassy Water*. Online. <<http://www.lsbu.ac.uk/water/amorph.html>>
- Source of Enceladus mosaic: <<http://solarsystem.dlr.de/Missions/cassini/intern/>>